

# Learning inducing points and uncertainty on molecular data

Mikhail Tsitsvero\*

*Institute for Chemical Reaction Design and Discovery  
Hokkaido University, Japan*

(Dated: July 20, 2022)

Uncertainty control and scalability to large datasets are the two main issues for the deployment of Gaussian process models into the autonomous material and chemical space exploration pipelines. One way to address both of these issues is by introducing the latent inducing variables and choosing the right approximation for the marginal log-likelihood objective. Here, we show that variational learning of the inducing points in the high-dimensional molecular descriptor space significantly improves both the prediction quality and uncertainty estimates on test configurations from a sample molecular dynamics dataset. Additionally, we show that inducing points can learn to represent the configurations of the molecules of different types that were not present within the initialization set of inducing points. Among several evaluated approximate marginal log-likelihood objectives, we show that the predictive log-likelihood provides both the predictive quality comparable to the exact Gaussian process model and excellent uncertainty control. Finally, we comment on whether a machine learning model makes predictions by interpolating the molecular configurations in high-dimensional descriptor space. We show that despite our intuition, and even for densely sampled molecular dynamics datasets, most of the predictions are done in the extrapolation regime.

## I. INTRODUCTION

Machine learning methods can significantly speed up the computational prediction of the physical and chemical properties of atomic systems by substituting the time-consuming electronic structure calculations with a surrogate predictive model. As predictive models for physical properties, such as energies and force fields, tend to become the active-learning components of the larger pipelines for material and chemical reaction design [1], [2], [3], it is essential for such models to autonomously reason about the uncertainty of predictions. Although significant progress has been made in designing the accurate models for approximating the potential energy surfaces [4], [5], [6], [7], [8], [9]; robust uncertainty control is still in an under-developed state to be suitable for a direct use in the systems with autonomous reasoning.

Uncertainty quantification is typically addressed within Bayesian worldview either by Bayesian model averaging, see e.g. [10], [11] or by directly learning the uncertainty parameters within the framework of Gaussian processes [12], [13], [14]. Here we follow the second route and address the problem of learning the uncertainty parameters by scalable Gaussian processes. For an extensive review and applications of Gaussian processes to material science and molecules, we refer the reader to [15].

Gaussian processes (GP) are often deemed the gold standard for many modeling applications, however, their application is hindered by scalability and over-estimation of the true uncertainty [16]. Variational methods in conjunction with stochastic training [17] aim to address the first issue, while designing the scalable approximations of the marginal log-likelihood objectives addresses the

second issue. In particular, inducing point methods [18] allow for scalable approximations to the exact GPs by introducing the learnable latent points variables that sparsify the GP model. Several scalable approximations of the marginal log-likelihood objectives were proposed recently [19], [16] that rely on bounding the model evidence and allowing to substitute the expensive-to-evaluate exact marginal log-likelihood objective.

In this paper, we first describe how the GP model can be augmented by the inducing points latent variables to achieve scalability. Then we present several options for approximating the marginal log-likelihood objective as well as outline options for modeling the variational distributions over the inducing variables. To illustrate the performance of the variational GP models with inducing points, we evaluate a collection of models with different setups, by fitting the potential energies of molecular configurations within a sample molecular dataset. The molecular dataset consists of a collection of short pieces of molecular dynamics trajectories for three structural isomers of a 12-atom molecule with test sets given by the continuations of molecular dynamics trajectories. We then evaluate the scalable GP models in terms of both the prediction quality on the test sets and the ability to separate the uncertainty on the training and test configurations.

Our key takeaways are the following: 1) learning the inducing points in high-dimensional molecular descriptor space significantly improves both the prediction quality and uncertainty estimates; 2) inducing points in the high-dimensional molecular descriptor space can learn to represent molecular configurations of different kinds of molecules; 3) among all the evaluated approximations of the marginal log-likelihood, the predictive log-likelihood objective [16] provides the best uncertainty separation jointly with high prediction quality.

In the last section, we briefly discuss whether a generic

---

\* e-mail: tsitsvero@gmail.com

machine learning model makes predictions on test configurations in high-dimensional descriptor space by interpolating within the training set of datapoints. By following the arguments by [20] we show, similarly to [21], that most test samples indeed fall outside of the convex hull of densely sampled training configurations in the continuous descriptor space; the phenomenon is due to the curse of dimensionality. Therefore we conclude that for most molecular datasets, a machine learning model that relies on some high-dimensional representation will always make predictions in the extrapolation regime.

## II. FITTING MOLECULAR DATA WITH SCALABLE GAUSSIAN PROCESSES

### A. Invariant Descriptors

To construct the rotation and translation invariant representations of atomic configurations in 3D space various methods were proposed where the data representation is either learned jointly with model parameters or constructed deterministically. Here we employ the widely used Smooth Overlap of Atomic Positions (SOAP) continuous and differentiable descriptors [22], [23]. We briefly describe the construction of the invariant vectors. The atomic structure  $\mathcal{A}$ , composed of atoms with atomic numbers  $Z$ , is described by the set of atomic positions  $\{\mathbf{R}_i\}_{i \in \mathcal{A}}$  with respect to some selected origin which we refer to as center. To build a representation of the entire atomic structure, we first select a collection of centers, capture the local environments around each center and combine them into global representation, see e.g. [24]. The local atomic structure can be mapped to Gaussian smooth atomic density by  $\rho^Z(\mathbf{r}) = \sum_i^{|Z_i|} e^{-1/2\sigma^2|\mathbf{r}-\mathbf{R}_i|^2} f_{cut}(\mathbf{r})$ , where  $f_{cut}$  is a cut-off function to consider only the atoms within short range  $[0, r_{cut}]$ . To build the simplest invariant representation vector, the atomic density is first projected onto the set of radial and spherical basis functions by

$$c_{nlm}^Z = \int_{\mathbb{R}^3} g_n(r) Y_{lm}(\theta, \phi) \rho^Z(\mathbf{r}) dV. \quad (1)$$

The simplest symmetry-invariant representation for a chosen center, referred to as SOAP power spectrum, is given by summation over the magnetic quantum number indices  $m$

$$p_{nn'l}^{Z_1 Z_2} = \pi \sqrt{\frac{8}{2l+1}} \sum_m \left( c_{nlm}^{Z_1} \right)^* \left( c_{n'l m}^{Z_2} \right). \quad (2)$$

As radial basis set one can choose, for example, the Gaussian Type Orbital (GTO) basis functions. Depending on the complexity of the molecular dataset and size of the atomic structures, only the expansion coefficients with radial and spherical indices of the orders up to  $n_{max}$  and  $l_{max}$  are considered. A simple way to build a vector representing the entire structure is just to average the local

power spectra over all the centers indexed by  $i$

$$\mathbf{x} \propto \sum_i \sum_m \left( c_{nlm}^{i, Z_1} \right)^* \left( c_{n'l m}^{i, Z_2} \right). \quad (3)$$

While we briefly described the simplest invariant representation that captures the 3-body correlations, a more expressive representation capturing higher order correlations sometimes is required, we refer the reader to [25] for a detailed review.

### B. Scalable Variational Gaussian processes

Gaussian processes offer rich non-parametric models for regression and classification tasks [26]. GP is fully specified by a mean function  $\mu : \mathbb{R}^d \rightarrow \mathbb{R}$  and kernel or covariance function  $k : \mathbb{R}^d \times \mathbb{R}^d \rightarrow \mathbb{R}$ . Choosing different kernel and mean allows to encode the prior information on the process that generated data. Typical example of kernel function that we will use in this paper is the scaled Radial Basis Function (RBF) kernel with Automatic Relevance Determination (ARD) [26]:

$$k(\mathbf{x} - \mathbf{x}' | \theta) = \theta_s \exp \left( -\frac{1}{2} \sum_{i=1}^d \frac{1}{\theta_i^2} (x_i - x'_i)^2 \right), \quad (4)$$

where  $\theta_s > 0$  is a scale parameter and  $\theta_i > 0$  are the lengthscale parameters; this type of kernel allows to assign short lengthscales over the irrelevant dimensions in descriptor space.

In the most common case of Gaussian likelihood, the predictive distribution of the target value  $y^*$  evaluated at the test location  $\mathbf{x}^*$  can be computed in closed form

$$p(y^* | \mathbf{x}^*) = \mathcal{N} \left( y^* | \mu_{\mathbf{f}}(\mathbf{x}^*), \sigma_{\mathbf{f}}(\mathbf{x}^*)^2 + \sigma_{\text{obs}}^2 \right), \quad (5)$$

where  $\sigma_{\text{obs}}$  is a learnable parameter representing the observation noise. Typically all the parameters of GP can be jointly learned with backpropagation by maximizing the marginal likelihood

$$p(\mathbf{y} | \mathbf{X}) = \int p(\mathbf{y} | \mathbf{f}, \sigma_{\text{obs}}^2) p(\mathbf{f} | \mathbf{X}) d\mathbf{f}, \quad (6)$$

where  $\mathbf{y}$  is the vector with real-valued targets,  $\mathbf{f}$  are the latent function values and  $\mathbf{X} = \{\mathbf{x}_i\}_{i=1}^N$  are the  $N$  input locations with  $\mathbf{x}_i \in \mathbb{R}^d$ . Unfortunately, expression (6) is too expensive to compute when number of training samples  $N$  is becoming large, since computation of the inverse of the kernel matrix  $\mathbf{K}_{NN}^{-1}$  scales as  $\mathcal{O}(N^3)$ , where  $\mathbf{K}_{NN} = k(\mathbf{X}, \mathbf{X})$ . This motivates the design of the approximate methods allowing for scalable GP inference.

Inducing point methods [27], [18], [28] offer a scalable extension for the exact GPs. The main idea behind the inducing point methods is to replace the large kernel matrix  $\mathbf{K}_{NN}$  with its low rank approximation  $\mathbf{K}_{MM}$  by introducing the latent variables  $\mathbf{u} \in \mathbb{R}^M$  which are evaluated over the set of  $M$  inducing points  $\mathbf{Z} = \{\mathbf{z}_m\}_{m=1}^M$ ,

with each  $\mathbf{z}_m \in \mathbb{R}^d$ . Inducing point locations may be set to be learnable variational parameters of the model. In this scenario the GP prior in (6) is replaced by

$$p(\mathbf{f} | \mathbf{X}) \rightarrow p(\mathbf{f} | \mathbf{u}, \mathbf{X}, \mathbf{Z})p(\mathbf{u} | \mathbf{Z}). \quad (7)$$

Using the Jensen’s inequality we can lower bound the log joint density over the targets and inducing variables

$$\begin{aligned} \log p(\mathbf{y}, \mathbf{u} | \mathbf{X}, \mathbf{Z}) &= \log \int p(\mathbf{y} | \mathbf{f})p(\mathbf{f} | \mathbf{u})p(\mathbf{u}) d\mathbf{f} \\ &\geq \mathbb{E}_{p(\mathbf{f}|\mathbf{u})}[\log p(\mathbf{y} | \mathbf{f}) + \log p(\mathbf{u})]. \end{aligned} \quad (8)$$

Finally, by introducing the variational distribution  $q(\mathbf{u})$  over the inducing variables, we come up with the following lower bounds for the evidence  $p(\mathbf{y})$  [29]

$$\begin{aligned} \log p(\mathbf{y}) &\geq \mathbb{E}_{q(\mathbf{u})}[\log p(\mathbf{y}, \mathbf{u} | \mathbf{X}, \mathbf{Z})] + H[q(\mathbf{u})] \\ &\geq \mathbb{E}_{q(\mathbf{u})} [\mathbb{E}_{p(\mathbf{f}|\mathbf{u})}[\log p(\mathbf{y} | \mathbf{f})]] - \text{KL}[q(\mathbf{u})\|p(\mathbf{u})], \end{aligned} \quad (9)$$

where  $H[q(\mathbf{u})]$  is an entropy term.

In the most common scenario, the variational distribution over the inducing variables  $\mathbf{u}$  is given by the multivariate normal  $q(\mathbf{u}) = \mathcal{N}(\mathbf{m}, \mathbf{S})$  parametrized by mean vector  $\mathbf{m} \in \mathbb{R}^M$  and covariance matrix  $\mathbf{S} \in \mathbb{R}^{M \times M}$ . Depending on the desired expressivity of the GP model and complexity of the data, we can choose to learn either the full positive semidefinite symmetric covariance matrix with non-zero non-diagonal elements, use the mean-field approximation by restricting  $\mathbf{S}$  to be diagonal, or even collapse the multivariate normal  $q(\mathbf{u})$  to a Dirac delta distribution by taking the formal limit  $\mathbf{S} \rightarrow 0$ .

Next we briefly present several objectives based on the Evidence Lower Bound (ELBO) (9) that allow for the scalable GP inference. Note how all three objectives will be naturally written as the sum of the data-fit term and the regularization term, thus explicitly targeting the model close to the desired prior  $p(\mathbf{u})$  that fits the observed data. Moreover all three objectives allow for data subsampling, therefore enabling to use the stochastic gradient-based optimization methods [17]. First, the approximate variational ELBO objective [28] is given by

$$\mathcal{L}_{\text{ELBO}} = \sum_{i=1}^N \mathbb{E}_{q(f_i)} [\log p(y_i | f_i)] - \beta \text{KL}[q(\mathbf{u})\|p(\mathbf{u})], \quad (10)$$

where  $q(f_i) := \int p(f_i | \mathbf{u}, \mathbf{x}_i) q(\mathbf{u}) d\mathbf{u}$  and  $\beta$  is a regularization parameter.

Another objective based on ELBO, referred to as  $\gamma$ -robust [19], aims at providing robustness to the training of GPs with respect to model misspecification and uncertainty control, where the log-likelihood term in ELBO is replaced with  $\gamma$ -divergence:

$$\begin{aligned} \mathcal{L}_\gamma &= \sum_{i=1}^N \mathbb{E}_{q(\mathbf{u})} \left[ -\frac{\gamma}{\gamma-1} \frac{p(y_i | \mathbf{u}, x_i)^{\gamma-1}}{\int p(y | \mathbf{u}, x_i)^\gamma dy} \right] \\ &\quad - \beta \text{KL}[q(\mathbf{u})\|p(\mathbf{u})], \end{aligned} \quad (11)$$

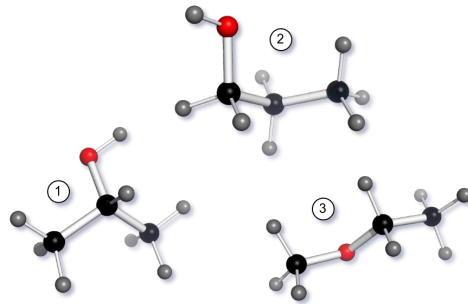


FIG. 1: Structural isomers of  $\text{C}_3\text{H}_8\text{O}$  molecule.

where  $\gamma$  is a hyperparameter and is set to be equal to 1.03 for the rest of the paper.

The third objective, proposed by [16], aims to improve the uncertainty estimates of the latent function, is referred to as the predictive log-likelihood and is given by

$$\mathcal{L}_{\text{PLL}} = \sum_{i=1}^N \log \mathbb{E}_{q(f_i)} [p(y_i | f_i)] - \beta \text{KL}[q(\mathbf{u})\|p(\mathbf{u})]. \quad (12)$$

For the presented objectives that approximate the evidence, we can calculate the derivatives efficiently and perform the training in a “black box” manner [30].

In all of the above approximations of ELBO, the accuracy term, which ensures fitness to the training data, is tightly balanced by the regularization term, which additionally makes the algorithm search for variational distributions with higher entropy, as can be seen from the first bound in (9). It is worth noting that the KL divergence term may also be replaced by the more general Rényi divergence [31], thus allowing for wider classes of variational distributions to be explored.

### III. LEARNING INDUCING POINTS

Although the training of the multiparametric variational GP model was cast in a “black box” manner, we still have to investigate carefully any of the possible pitfalls. One possible problem is the initialization of the inducing points. For example, we found that the optimization of the components of high-dimensional inducing point vectors, initialized by random draws from the normal distribution  $\mathcal{N}(0, 1)$ , is typically stuck in a local minimum and the trained model performs poorly. Therefore proper initialization of inducing point vectors is needed. In this section, first, we demonstrate that learning the inducing points significantly improves prediction quality and, second, that inducing points initialized on one kind of molecule can learn to represent different kinds of molecules.

Our claim is that learning the inducing points can largely improve the prediction quality, especially on the

configurations that have not been represented by the initialization selection of data points from the training set. We proceed with the example of fitting the potential energies of the conformations from the molecular dynamics trajectories of molecules from Fig. 1 with a collection of variational GPs. For each molecule, we generated a short 20 ps molecular dynamics trajectory at 300 K temperature with GFN2-xTB tight-binding Hamiltonian [32]. Trajectories were calculated with 0.4 fs time step, and then subsampled to 10 fs time step [33]. After subsampling each trajectory consisted of 2000 snapshots. We then selected the first 1600 configurations within each trajectory to be included in a training dataset, while the remaining 400 configurations within each trajectory, were selected for test sets. In total, the training set consists of 4800 configurations and there are three test sets with 400 configurations each. For each configuration of test/train sets, we computed the 720-dimensional invariant SOAP vector representation (3) with [34]. For this paper the invariant vectors were computed with the following parameters:  $n_{max} = 5$ ,  $l_{max} = 5$ ,  $r_{cut} = 5.0 \text{ \AA}$  and  $\sigma = 0.5 \text{ \AA}$ . Four atoms, namely the three carbons and the oxygen, were selected as centers for calculating the invariant vectors by Eq. (3).

Regarding the number of additional variational parameters, if one chooses for example to learn 1000 inducing points, it will amount to additional 720 000 variational parameters corresponding to the inducing point vectors’ components. As discussed in detail in Section V, this kind of dataset intrinsically is not that high-dimensional – the variability of the data can be captured by only several dozen PCA singular vectors. With random inducing point initialization, the gradient descent might simply fail to locate the relevant subspace and then navigate within it to obtain the optimal solution. To check how the inducing points  $\mathbf{Z}$  can migrate during the training to represent different types of molecules, we initialized inducing points by randomly sampling the configurations only of the first molecule.

The target values  $\mathbf{y}$  that we aim to fit with GP models are the potential energies of molecules. The difference between the maximum and minimum energies of configurations within the training set (including all three molecules) is 0.8036 eV, thus we normalized the energies to fall into the interval  $[0, 1]$  by scaling with this number. In the diagrams, we show the error metrics in the normalized units. Our goal here is not to reach the ultimate accuracy, but to illustrate the concept, while for the ultimate accuracy one may need to calculate the invariant descriptors with a greater number of radial and spherical basis functions, design the optimal shape of the cutoff function, choose optimal values of  $\sigma$ , as well as design more efficient ways to combine the local invariants, other than summation (3) – a separate set of problems.

To compare the different variational GP models and training strategies given in the previous section, we built a collection of  $3 \times 3 \times 3 \times 2 = 54$  models corresponding to: three objective functions given by the ELBO ap-

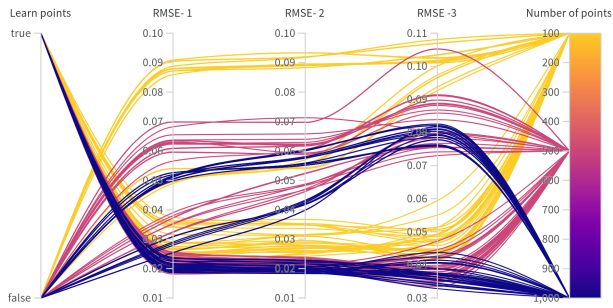


FIG. 2: Performance results of the variational GP training. Learning of the inducing points provide lower errors on all three test sets and for all variational setups.

proximations by Eqs. (10), (11) and (12); three types of normal variational distributions, one with learning the full covariance matrix, one with diagonal covariance (mean-field approximation), and one with delta covariance, where only the mean vector of the normal distribution is learned; three numbers of inducing points of 100, 500 and 1000 points; two regimes defining on whether the inducing point vector components are learnable parameters or not. Each of the 54 models were run 3 times to ensure the stability of convergence. Empirically we found little dependence of the learning quality and uncertainty estimates on varying the regularization parameter  $\beta$  within the approximations of ELBO for this dataset and we used  $\beta = 0.1$  in all the experiments. Additional information on the training procedure is given in the Supplementary Information.

In Fig. 2, in the parallel coordinates chart, we show the performance of various GP models in terms of the Root Mean Square Error (RMSE) evaluated on each of the three test sets. We can make several observations. First, we observe that learning the inducing points significantly improves the performance of the variational GP models. We recall that inducing points were initialized only by the configurations of the first molecule with corresponding test RMSE-1 in Fig 2. The gain in the prediction performance by learning the inducing points is greater for the low number of inducing points, which could be simply because too few initial inducing configurations failed to represent a large part of the training dataset while introducing additional  $100 \times 720 = 72000$  parameters within the model makes it much more expressive. The second observation is that, although the inducing points were initialized by the configurations of the first molecule, the learned high-dimensional inducing point vectors represent well the different configurations of the second and third molecules. The learned inducing points vectors could parsimoniously “entangle” the invariant vectors of different types of molecules across different dimensions, thus making the whole model more expressive.

One immediate application for learning the inducing

points would be the selection of a representative subset of molecular configurations. We can easily build a variational GP model that iteratively updates batches of inducing points parameters with corresponding subsets of training configurations which they aim to represent; note that all three objectives (10), (11) and (12) allow for data subsampling making it possible to update gradients for batches of parameters with respect to batches of data points. After training such a model, we can select only the configurations that are closest in covariance metric to the learned inducing points. Such selection of configurations will be automatically supported by the predictive power of the trained GP, in contrast to the approaches such as “farthest point sampling” or based on matrix factorizations, see [24] for details. Otherwise, one can combine the sparsely selected representative structures with inducing points learning, thus automatically adjusting the inducing point vectors to represent the configurations that were under-represented by the initial representative set.

#### IV. LEARNING UNCERTAINTY

In all three objectives given by eq. (10), (11) and (12) the variance of the prediction  $y^*$  evaluated at the test point  $\mathbf{x}^*$  is given by the sum of the global observation noise parameter  $\sigma_{\text{obs}}^2$  and the local latent function variance  $\sigma_{\mathbf{f}}(\mathbf{x}^*)^2$ :

$$\text{Var}[y^* | \mathbf{x}^*] = \sigma(\mathbf{x}^*)^2 := \sigma_{\text{obs}}^2 + \sigma_{\mathbf{f}}(\mathbf{x}^*)^2. \quad (13)$$

As pointed out in [16], the variational ELBO (10) and  $\gamma$ -robust (11) objectives tend to underestimate the latent function variance by attributing most of the uncertainty to the global observation noise  $\sigma_{\text{obs}}^2$ . This is because the data fit term in (10) contains the term proportional to  $\frac{1}{\sigma_{\text{obs}}^2} |y_i - \mu_{\mathbf{f}}(\mathbf{x}_i)|^2$ , while in the predictive log-likelihood objective the data fit term contains the term proportional to  $\frac{1}{\sigma_{\text{obs}}^2 + \sigma_{\mathbf{f}}(\mathbf{x}_i)^2} |y_i - \mu_{\mathbf{f}}(\mathbf{x}_i)|^2$ , thus equilibrating the scales of the learned global and local contributions to variance.

We now illustrate the impact the different variational settings have on learning the variance on the same dataset of configurations of three molecules as in the previous section. To check how well the model can distinguish uncertainties on the train and test datasets, we introduce a simple metric that measures the ratio of the mean variance on the training subset of configurations  $T$  to the mean variance on the test subset of configurations  $S$ :

$$R(T, S) = \frac{|S| \sum_{i \in T} \sigma(\mathbf{x}_i^*)^2}{|T| \sum_{j \in S} \sigma(\mathbf{x}_j^*)^2}. \quad (14)$$

We then evaluate the same variational setup as described in the previous section. By denoting the  $T_1$ ,  $T_2$ ,  $T_3$  and  $S_1$ ,  $S_2$ , and  $S_3$  the training and test subsets of

configurations corresponding to the first, second, and the third molecule, we compute the ratios  $R_i = R(T_i, S_i)$ . We have chosen the test sets to contain the continuations of the trajectories because, on the one hand, test configurations are somewhat similar to the subset of training configurations, therefore making predictions on them makes sense, on the other hand, test configurations should still be different from the training configurations because they lie outside of the intervals of short molecular dynamics trajectories, and, therefore, measuring uncertainty is also reasonable for them.

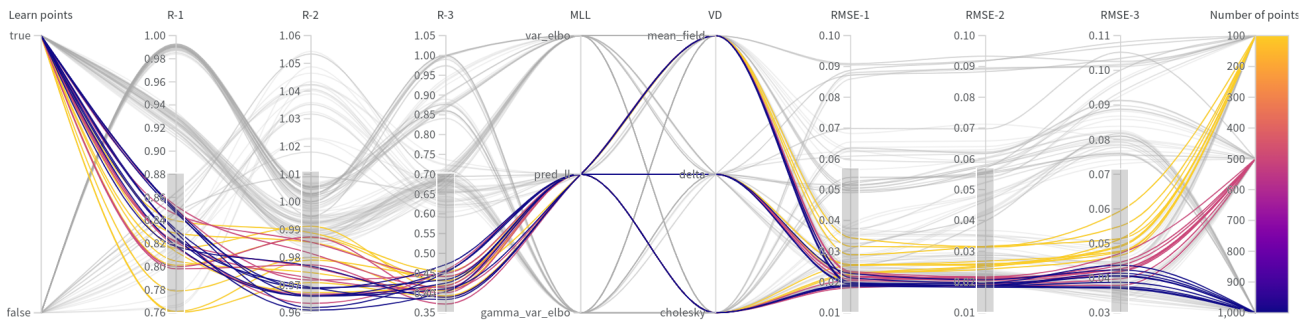
In Fig. 3 (a), we provide the results of experiments, where for ease of perception we highlighted the lowest variance ratios jointly with the lowest RMSE metrics to see what kind of variational setting performs well on both measures for all test and train subsets. We can observe that the predictive log-likelihood objective (12) allowed to balance the prediction power of the model with a sharper separation between the mean variances on test and train configurations. Quite differently from the choice of the objective to minimize, we found that different variational distributions performed similarly.

Next, in the Fig. 3 (b), we highlighted the curves corresponding to the fixed number of 1000 inducing points and the predictive log-likelihood objective. We can observe that learning inducing points allowed to significantly reduce the RMSE-1 error from 0.25 to 0.19, in other words, the prediction error on the first molecule trajectory from which the inducing points were initialized. This may seem initially striking since now part of the inducing points have to migrate toward configurations of the other two molecules, however, we must remind ourselves that we are fitting a probabilistic model having hundreds of thousands of parameters, and the model is just able to separate data points better. We pay a price in terms of computations for finer uncertainty control and prediction quality.

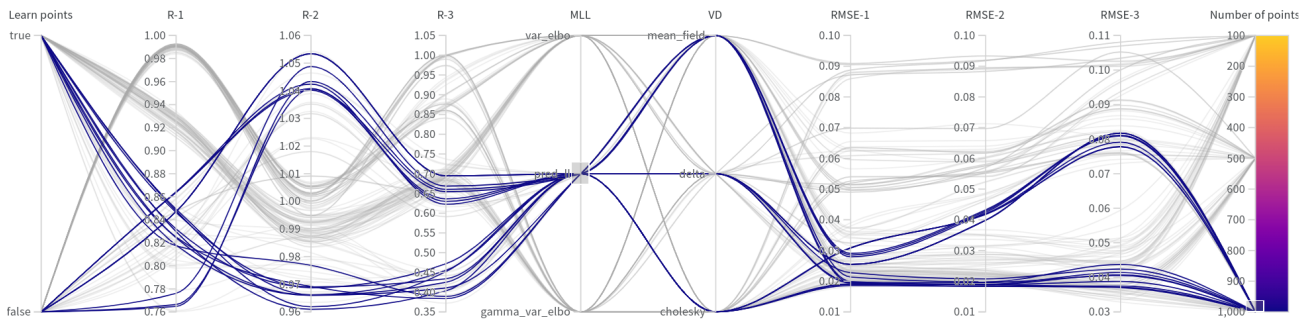
Mol., $i$	RMSE- $i$	$R(T_i, S_i)$
1	0.016	0.96
2	0.019	0.95
3	0.040	0.91

TABLE I: Performance of GP model trained with exact marginal log-likelihood.

For comparison, in Table I, we also report the prediction quality and ratio of mean variances for the exact inference, where the GP uses all training points for inference and is trained by maximizing the exact marginal log-likelihood (6). The comparison with exact GP is striking, since learning the inducing points allowed to improve the separation of train/test uncertainties while at the same time retained the prediction quality of the model almost at the level of the exact GP model. Overestimated uncertainty, when training GP models with exact marginal log-likelihood objective, is a known issue, see e.g. [14] and [26]. Variational GP model with inducing points and with proper scalable objective, such as the predic-



(a) Best separation of uncertainties and lowest errors



(b) Predictive log-likelihood objective and 1000 inducing points

FIG. 3: Parallel coordinates chart showing the relative mean train/test uncertainty ratios and test errors for three marginal log-likelihood (MLL) loss functions, three variational distributions (VD) and evaluated for 100, 500 and 1000 inducing points. In (a) the runs with the lowest train/test mean variances ratios and the lowest RMSE are highlighted. Each combination of parameters was run 3 times to ensure the stability of convergence.

tive log-likelihood, therefore allowed us to improve the uncertainty estimates almost without sacrificing the predictive quality. The price we pay for the finer uncertainty control is again computational. When training the multi-parametric variational model, we had to carefully choose the gradient step size and increase the number of training epochs. For example, the variational models were trained with 20 000 epochs with varying step sizes (see the Supplementary Information for details), while for the training of a simple GP model with exact marginal log-likelihood objective, typically, several hundreds of epochs suffice.

## V. INTERPOLATION VS. EXTRAPOLATION

It is often silently assumed that Gaussian processes make the predictions on the test data points by interpolating within the training set of points, which is mostly an obvious statement for low-dimensional datasets. At the same time, looking at the simulations of the molecular dynamics of small molecules, like the ones from Fig. 1, makes us think that conformational diversity during dynamics is quite restricted – if some test snapshot is

taken in between two closely sampled in time neighboring snapshots, in some intuitive sense it “interpolates” between its neighbors. Hence, if we want to predict some physical property, like potential energy, for a collection of test configurations, we might be lured into thinking that the machine learning algorithm will *interpolate in between* the training configurations also in the descriptor space. By “in between,” it is typically assumed that a test point will be within the convex hull of the training points. Here we follow the arguments by [20], where it was shown that for high-dimensional datasets, like the image data, learning always amounts to extrapolation. Recently, a similar kind of analysis was performed on typical molecular datasets [21], where authors additionally propose an alternative protocol to quantify the similarity of a test point to the training set of points based on the estimated density of training points.

Next, we demonstrate, similarly to [20] and [21], that for the molecular dynamics datasets with high-dimensional descriptor representations like SOAP, the situation is quite similar, even if we form the dataset by very similar molecular configurations, the randomly sampled test configuration descriptor vector will most likely fall outside the convex hull of the training set of points.

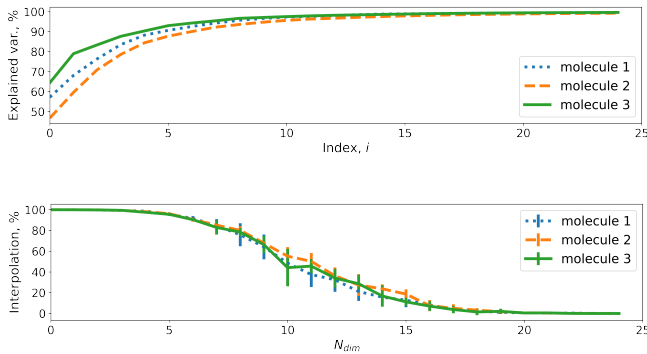


FIG. 4: (a) Fraction of the total variance explained by the first  $i$  singular vectors. (b) Fraction of points from the test set within the convex hull of the training points for random selections of  $N_{dim}$  dimensions; the standard deviations across the runs are shown with vertical bars.

This phenomenon is a direct consequence of the curse of dimensionality, it clearly shows that the meaning of interpolation and extrapolation needs to be properly adjusted to the problem at hand when addressing problems in higher dimensions and alternative similarity measures need to be constructed [21].

We illustrate this phenomenon on a simple molecular dataset given by the molecular dynamics trajectories of the molecules from Fig. 1. As before, for these molecules, we generated a large set of conformations simply by simulating a 100 ps molecular dynamics trajectories at 300 K temperature using the same parameters and method as in the previous section. To get an estimate of the variability of the invariant vectors within the dataset, we applied the Principal Component Analysis (PCA) to the dataset containing invariant vectors for 10 000 consecutive snapshots. In Fig. 4 (a), we illustrate what fraction of the total variance is explained by the first  $i$  largest singular values  $\sigma_j$ , i.e., we plot  $r_i = \sum_{j=0}^{i-1} \sigma_j^2 / \sum_{j=0}^{d-1} \sigma_j^2$ . For example, the first 15 principal components explain 96.5%, 94.7% and 97.1% of total variance for the first, the second, and the third molecule.

Next, we show what fraction of test points falls within the convex hull of training points for randomly selected subspaces in the descriptor space. First, we formed a randomized collection of test vectors by randomly selecting 200 configurations from the pool of 10 000 configurations corresponding to the 100 ps trajectory for each molecule. Then for a collection of train and test vectors, we randomly subsampled  $N_{dim}$  dimensions.

Constructing the convex hull for high-dimensional datapoints is computationally expensive, however, checking hull membership for a test point can be cast as a

linear programming problem with positivity constraints. By successfully solving the linear program we can check whether a test point can be represented by a linear combination of the training points with positive weights summing up to one.

In Fig. 4 (b), we illustrate what fraction of test points falls within the convex hull of the training points for randomly sampled  $N_{dim}$  dimensions in the descriptor space. For each number of dimensions  $N_{dim}$  we made 10 runs with different random selections of test configurations and dimensions for random projections. To conclude, we see that due to the curse of dimensionality, in the full high-dimensional descriptor space, only a small fraction of predictions will be performed in the interpolation regime.

## VI. DISCUSSION

In this work, we presented the general setting for scalable Gaussian processes and applied it to a molecular dataset. Our experiments clearly showed that introducing and learning the latent inducing variables in a high-dimensional molecular descriptor space with a proper approximate marginal log-likelihood objective improved both prediction quality and uncertainty estimates. It was demonstrated that during the training, the model can learn to represent different types of molecular configurations that were not present within the initialization set of inducing points.

Although augmenting a GP model with a large number of variational parameters clearly showed its advantages, it also made the training process more complex. Moreover, even though the learned inducing points could represent different types of configurations, their proper initialization was necessary, and the extent to which inducing points can adapt to represent different molecular configurations is still unexplored. These issues are tightly related to the currently available methods to accelerate the training of variational parameters, such as “whitening” [35], that was used in this work, and the choices of the molecular descriptor representations such as SOAP. In future work, we aim to address the above issues as well as apply variational multiparametric GP models to a variety of large-scale problems.

## ACKNOWLEDGMENTS

The author wishes to acknowledge the various fruitful discussions within the group of Prof. T. Komatsuzaki that immensely contributed to this work.

[1] L. Sbailò, Á. Fekete, L. M. Ghiringhelli, and M. Scheffler, The nomad artificial-intelligence toolkit: Turning

materials-science data into knowledge and understand-

- ing, arXiv preprint arXiv:2205.15686 (2022).
- [2] J. P. Unslieber, S. A. Grimmel, and M. Reiher, Chemoton 2.0: Autonomous exploration of chemical reaction networks, arXiv preprint arXiv:2202.13011 (2022).
  - [3] S. Maeda, Y. Harabuchi, M. Takagi, T. Taketsugu, and K. Morokuma, Artificial force induced reaction (afir) method for exploring quantum chemical potential energy surfaces, *The Chemical Record* **16**, 2232 (2016).
  - [4] A. P. Bartók, M. C. Payne, R. Kondor, and G. Csányi, Gaussian approximation potentials: The accuracy of quantum mechanics, without the electrons, *Physical review letters* **104**, 136403 (2010).
  - [5] J. Vandermause, Y. Xie, J. S. Lim, C. J. Owen, and B. Kozinsky, Active learning of reactive bayesian force fields: Application to heterogeneous hydrogen-platinum catalysis dynamics, arXiv preprint arXiv:2106.01949 (2021).
  - [6] S. Chmiela, A. Tkatchenko, H. E. Sauceda, I. Poltavsky, K. T. Schütt, and K.-R. Müller, Machine learning of accurate energy-conserving molecular force fields, *Science advances* **3**, e1603015 (2017).
  - [7] S. Chmiela, H. E. Sauceda, K.-R. Müller, and A. Tkatchenko, Towards exact molecular dynamics simulations with machine-learned force fields, *Nature communications* **9**, 1 (2018).
  - [8] S. Chmiela, H. E. Sauceda, I. Poltavsky, K.-R. Müller, and A. Tkatchenko, sGDML: Constructing accurate and data efficient molecular force fields using machine learning, *Computer Physics Communications* **240**, 38 (2019).
  - [9] K. T. Schütt, S. Chmiela, O. A. von Lilienfeld, A. Tkatchenko, K. Tsuda, and K.-R. Müller, Machine learning meets quantum physics, *Lecture Notes in Physics* (2020).
  - [10] M. Wen and E. B. Tadmor, Uncertainty quantification in molecular simulations with dropout neural network potentials, *npj Computational Materials* **6**, 1 (2020).
  - [11] G. Imbalzano, Y. Zhuang, V. Kapil, K. Rossi, E. A. Engel, F. Grasselli, and M. Ceriotti, Uncertainty estimation for molecular dynamics and sampling, *The Journal of Chemical Physics* **154**, 074102 (2021).
  - [12] F. Musil, M. J. Willatt, M. A. Langovoy, and M. Ceriotti, Fast and accurate uncertainty estimation in chemical machine learning, *Journal of chemical theory and computation* **15**, 906 (2019).
  - [13] G. N. Simm and M. Reiher, Error-controlled exploration of chemical reaction networks with gaussian processes, *Journal of chemical theory and computation* **14**, 5238 (2018).
  - [14] A. P. Bartók, J. Kermode, *et al.*, Improved uncertainty quantification for gaussian process regression based interatomic potentials, arXiv preprint arXiv:2206.08744 (2022).
  - [15] V. L. Deringer, A. P. Bartók, N. Bernstein, D. M. Wilkins, M. Ceriotti, and G. Csányi, Gaussian process regression for materials and molecules, *Chemical Reviews* **121**, 10073 (2021).
  - [16] M. Jankowiak, G. Pleiss, and J. Gardner, Parametric gaussian process regressors, in *International Conference on Machine Learning* (PMLR, 2020) pp. 4702–4712.
  - [17] M. D. Hoffman, D. M. Blei, C. Wang, and J. Paisley, Stochastic variational inference, *Journal of Machine Learning Research* (2013).
  - [18] M. Titsias, Variational learning of inducing variables in sparse gaussian processes, in *Artificial intelligence and statistics* (PMLR, 2009) pp. 567–574.
  - [19] J. Knoblauch, Robust deep gaussian processes, arXiv preprint arXiv:1904.02303 (2019).
  - [20] R. Balestriero, J. Pesenti, and Y. LeCun, Learning in high dimension always amounts to extrapolation, arXiv preprint arXiv:2110.09485 (2021).
  - [21] C. Zeni, A. Anelli, A. Glielmo, and K. Rossi, Exploring the robust extrapolation of high-dimensional machine learning potentials, *Physical Review B* **105**, 165141 (2022).
  - [22] A. P. Bartók, R. Kondor, and G. Csányi, On representing chemical environments, *Physical Review B* **87**, 184115 (2013).
  - [23] S. De, A. P. Bartók, G. Csányi, and M. Ceriotti, Comparing molecules and solids across structural and alchemical space, *Physical Chemistry Chemical Physics* **18**, 13754 (2016).
  - [24] M. Ceriotti, M. J. Willatt, and G. Csányi, Machine learning of atomic-scale properties based on physical principles, *Handbook of Materials Modeling: Methods: Theory and Modeling*, 1911 (2020).
  - [25] M. J. Willatt, F. Musil, and M. Ceriotti, Atom-density representations for machine learning, *The Journal of chemical physics* **150**, 154110 (2019).
  - [26] C. K. Williams and C. E. Rasmussen, *Gaussian processes for machine learning*, Vol. 2 (MIT press Cambridge, MA, 2006).
  - [27] E. Snelson and Z. Ghahramani, Sparse gaussian processes using pseudo-inputs, *Advances in neural information processing systems* **18** (2005).
  - [28] J. Hensman, N. Fusi, and N. D. Lawrence, Gaussian processes for big data, arXiv preprint arXiv:1309.6835 (2013).
  - [29] J. Hensman, A. Matthews, and Z. Ghahramani, Scalable variational gaussian process classification, in *Artificial Intelligence and Statistics* (PMLR, 2015) pp. 351–360.
  - [30] R. Ranganath, S. Gerrish, and D. Blei, Black box variational inference, in *Artificial intelligence and statistics* (PMLR, 2014) pp. 814–822.
  - [31] J. Knoblauch, J. Jewson, and T. Damoulas, Generalized variational inference: Three arguments for deriving new posteriors, arXiv preprint arXiv:1904.02063 (2019).
  - [32] C. Bannwarth, S. Ehlert, and S. Grimme, GFN2-xTB—an accurate and broadly parametrized self-consistent tight-binding quantum chemical method with multipole electrostatics and density-dependent dispersion contributions, *Journal of chemical theory and computation* **15**, 1652 (2019).
  - [33] M. Tsitsvero, Molecular dynamics trajectories of C3 H8 O molecule and its structural isomers, 10.5281/zenodo.6496747 (2022).
  - [34] L. Himanen, M. O. J. Jäger, E. V. Morooka, F. Federici Canova, Y. S. Ranawat, D. Z. Gao, P. Rinke, and A. S. Foster, DScribe: Library of descriptors for machine learning in materials science, *Computer Physics Communications* **247**, 106949 (2020).
  - [35] A. G. d. G. Matthews, *Scalable Gaussian process inference using variational methods*, Ph.D. thesis, University of Cambridge (2017).